The Designs and Testing of Biodegradable Inserts for Enhanced Crashworthiness in Sports Helmets

Paweł Kaczyński , Mateusz Skwarski * , Anna Dmitruk , Piotr Makuła , Joanna Ludwiczak

Posted Date: 15 August 2024

doi: 10.20944/preprints202408.1139.v1

Keywords: honeycomb; biodegradable polymers; material models; mechanical properties; FEM; tensile test; dynamic test; crashworthiness

 doi:10.20944/preprints202408.1139.v1

Article

The Designs and Testing of Biodegradable Inserts for Enhanced Crashworthiness in Sports Helmets

Paweł Kaczyński [1], Mateusz Skwarski [1,*], Anna Dmitruk [2], Piotr Makuła [1] and Joanna Ludwiczak [3]

[1] Wroclaw University of Science and Technology, Faculty of Mechanical Engineering, Department of Metal Forming Welding and Metrology, Wybrzeze Wyspianskiego 27, 50-370, Wroclaw, Poland; pawel.kaczynski@pwr.edu.pl, piotr.makula@pwr.edu.pl

[2] Wroclaw University of Science and Technology, Faculty of Mechanical Engineering, Department of Lightweight Elements Engineering, Foundry and Automation, Wybrzeze Wyspianskiego 27, 50-370, Wroclaw, Poland; anna.dmitruk@pwr.edu.pl

[3] Wroclaw University of Science and Technology, Faculty of Environmental Engineering, Department of Environmental Protection Engineering, Wybrzeze Wyspianskiego 27, 50-370, Wroclaw, Poland; joanna.ludwiczak@pwr.edu.pl

* Correspondence: mateusz.skwarski@pwr.edu.pl

Abstract: The article addresses manufacturing structures made of biodegradable materials that can be successfully used as energy absorbing liner of sports helmets of all kinds, replacing the previously used expanded polystyrene. The paper is focused on injection technological tests and tensile tests (in quasi-static and dynamic conditions) of several composites based on a PLA matrix with the addition of other biodegradable softening agents, such as PBAT and TPS. Next, the thin walled elements (dimensions of 55 x 55 x 20 mm) were manufactured and evaluated using a spring-loaded drop hammer. The 60J impact energy was tested according to EN 1078 standard. The dynamic crushing testing included checking the influence of the materials temperature (-20, 0, 20, and 40 °C) and the impact velocity. The PLA15PBAT85 blend was selected as the most effective material in terms of its use as energy absorbing liner for sport helmets.

Keywords: honeycomb; biodegradable polymers; material models; mechanical properties; FEM; dynamic test; crashworthiness

1. Introduction

Energy absorption applications (e.g. in automotive, aerospace, architecture, sport and leisure, biomedical sectors) utilize various kinds of materials such as e.g. composites, hybrid materials, polymer or metallic foams, cellular structures like honeycombs or complex hierarchical systems [1–4]. Multi-cell thin-walled systems are the ones most commonly applied [5]. Usually, the overall aim is for the material to be durable and possess low mass at the same time, what widens the necessity to rely on polymers or lightweight metal alloys. Moreover, such elements should be affordable in terms of production and exploitation costs. Thin-walled cellular shapes offer not only low mass but also tailorable mechanical and energy absorption properties, adjustable by variable cell size, orientation, cross-section or wall thickness. Such materials, often applied in the form of a core in a sandwich arrangement, exhibit various destruction mechanisms, depending on their orientation towards the working load. For example, honeycombs compressed in a direction perpendicular to their walls (in-plane compression) behave quite similarly as metallic foams, as their deformation proceeds based on the local densification up to the point where the open cells are no longer present and the structure starts to perform as a solid body [6–8]. The main difference between these structures is connected with the fact that pores of the foam collapse rather evenly in the whole volume, while honeycombs tend to deform gradually – e.g. in row after row sequence [9]. On the other hand, if utilized aligned with the main direction (out-of-plane compression) in accordance with the cells' elongation,

 doi:10.20944/preprints202408.1139.v1

honeycombs act differently – the energy absorption performance is the most beneficial, because of the enhanced load-bearing ability, especially with the use of thin-walled structures that enables the plastic deformation by folding. Regular honeycombs can be turned into more advanced solutions for example by combining them with other geometries in hierarchical shapes, making them multimaterial, irregular or density-graded [10] (with changeable cell size or wall thickness). Among other bio-inspired spatial constructs, the following can be distinguished: nacre, conch shell, shrimp shell, horns, hooves, spiderweb, beetle wings, bones, bamboo, fish scales, pomelo, horseshoe or crocodile skin etc. [1,11,12]. Structural foams of open or closed porosities are equally often used as energy absorbers as honeycombs. Avalle et al. [13] tested energy absorption characteristics during static or dynamic deformation of three polymeric foams: expanded polypropylene (EPP), rigid polyurethane foam (PUR) and blend of polyamide with modified polyphenylene and polystyrene (NORYL GTX®). PUR foams perform in a comparable manner independently from the strain rate and their deformation is permanent, therefore it cannot withstand multiple impacts. Polypropylene- and polyamide-based foams exhibit similar behavior to each other – strongly dependent on the strain rate. Their energy absorption efficiency and absorber energy are higher for dynamic tests than for static ones and increase together with the relative density of the sample. It can be concluded that it is crucial for the energy absorbing materials to be simultaneously durable and ductile to some extent. In this work, where emphasis was put on designing materials solution for replaceable, biodegradable cores for protective sports helmets, this direction was a leading one.

Modern techniques are widely applied for designing and manufacturing of complex shapes. For example, additive manufacturing offers the possibility to change the material during 3D printing, what allows to print multimaterial honeycomb, like the ones composed of ABS and TPU, that were described by Khatri and coauthors [14]. Proposed structures were easily tunable by controlling of the thickness of particular layers. Kumar et al. [15] fabricated 3D-printed cellular structures from TPU, both with open and closed porosity, which were suggested to be used as energy absorbers in midsole shoes. Recently, also auxetic structures have drawn the attention of researchers [16]. Gunaydin and coauthors [17] tested their compressive and energy absorption behaviors for several material options (nylon, composite of nylon and carbon fiber, composite of nylon and glass fiber) and found them to be even more effective than common hexagons. Apart from auxetic structures (otherwise called re-entrant) also honeycombs with chiral architecture made by additive manufacturing from UV curable resin were tested by Kumar et al. [18]. Anti-chiral and origami PLA structures were analyzed by Mehrpouya and coauthors [19], focusing on maximizing energy absorption characteristics in sandwich materials. Ha et al. [20] studied circular hierarchical honeycombs characterized by improved relative stiffness, strength and energy absorption properties. Another new approach was reported by Wu et al. [21], who investigated hierarchical thin-walled structures based on space-filling Moore curves differing in relative density and order. Hybrid materials for energy absorption can also combine areas of metal foundry and plastics processing, as was described by Peixinho et al. [22], who reported a manufacturing route and performance analysis for aluminum spatial structures produced by investment casting joined with polymer (PP or ABS) fillings. A similar solution was investigated by Diamantopoulou and coauthors [23], by utilizing polymer core and ceramics (alumina) as a lattice. Metallic shells can be also applied as tubes (aluminum or steel) filled with orderly arranged cellular or foam-like polymer cores [24,25]. There are also attempts to fill honeycomb cells interiors with various porous patterns. Ragab and coauthors [26] designed and manufactured by 3D printing PLA honeycombs with infill of Voronoi tesselations that were characterized by superior mechanical and energy absorption properties in comparison to regular hexagonal structures. Their energy absorption, crash force efficiency and specific energy absorption belonged to the range of, respectively, 350 to 435 J, 1.42 to 1.65 and 1.60 to 1.82 J/g. Other 3D-printed patterns (polyamide-12, polylactide, photopolymer), similar to Voronoi, that were tested in terms of energy absorption are Schwartz primitive, diamond, neovious, I-WP, gyroid [27]. Gisario et al. [28] evaluated different cellular topologies for PLA custom-designed fittings for energy absorption and damping usage: lozenge, tetrachiral, anittetrachiral, rototetrachiral, hexachiral, rotochiral. Octet-truss cells were also considered by Bolan et al. [29]. All of the listed examples highlight the necessity to use advanced

 doi:10.20944/preprints202408.1139.v1

cross-sections with high level of complexity to ensure that the requirements for elements exposed to possible impacts during operation are met, which entails inevitability to engage expensive, time-consuming manufacturing methods. In this paper a contrary approach was undertaken aiming to simplify the structure and the production process, assuring the satisfactory mechanical and energy absorption performance by creating a dedicated polymer blend and utilizing plastic folding deformation mechanism in thin-walled cellular constructs to be used as cores in protective sports helmets. Biodegradability and replaceability were another key factors considered for this purpose.

Today, the development of biodegradable polymers has gained significant attention as a promising solution to address the environmental concerns associated with conventional plastics. Biodegradable polymers, also known as biopolymers, are designed to break down naturally over time (e.g. maximum of 6 months), reducing their impact on ecosystems and minimizing pollution [30]. Trials of manufacturing of biodegradable polymeric foams composed of modified castor oil, styrene and isobornyl methacrylate were described by Dicks et al. [31]. Biodegradable polymeric structures proposed in this paper as replaceable cores for protective sports helmets have several advantages. First, users can easily replace them after a crash, restoring 100% of the helmet's protective properties. Second, these structures can be disposed of by composting. Third, they provide better protective properties because they utilize a previously unused mechanism of plastic folding instead of compression of polystyrene elements, for which the deformation mechanism is the one typical for foam-like materials, as polystyrene beads (cells) densify and collapse near the place of the applied load [32]. Plastic deformation, beneficial for maximization of energy absorption, can be introduced by buckling initiators [33] or, as hereby in the proposed approach, by blending various materials to ensure obtaining desired mechanical properties.

2. Materials and Methods

2.1. Determination of Plasticizing Curves

The materials used during the tests were based on PLA matrix (PLI 005, NaturePlast) with the addition of softening biodegradable plastics such as PBAT (Ecoflex F Blend C1200, BASF) and TPS (a starch-based biopolymer, MaterBi EF03A0, Novamont). The mechanical properties of base materials are briefly presented in Table 1. The blends were prepared by melt blending using a twin-screw extruder (Haake PolyLab QC, Thermo Scientific). The following mass compositions were prepared: PLA50TPS50, PLA30TPS70, PLA15TPS85, PLA50PBAT50, PLA30PBAT70, PLA15PBAT85. After the extrusion process, the materials were cooled and granulated. Next, the granules were used to produce specimens for tensile testing and energy-absorbing structures (inserts) by injection molding with the use of Demag Ergotech Compact 50-120 injection molding machine.

Table 1. Material properties of PLA, PBAT and TPS.

Material	Ultimate tensile strength [MPa]	Maximum elongation [%]
PLA	60-70	7-8
PBAT	14-20	570-740
TPS	12-15	560-580

For the purpose of strength testing 4 mm thick, flat specimens were prepared and manufactured by injection molding. Typical geometry defined by the ISO 3167:2002-02 standard (Figure 1a) was used for tests conducted in the quasi-static conditions (strain rates of 0.01 and 0.1 s^{-1} were selected). Tensile tests were carried out on a TINIUS OLSEN H25KT testing machine.

 doi:10.20944/preprints202408.1139.v1

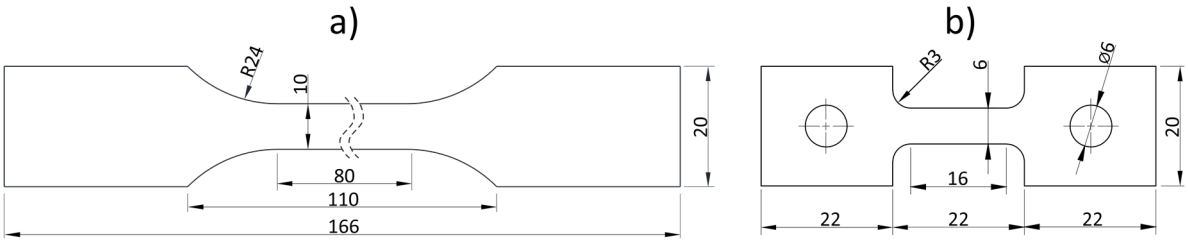

Figure 1. Geometry of samples used for tensile tests: a) quasi-static tests; b) dynamic tensile tests.

Samples with reduced dimensions (Figure 1b) were used for dynamic tensile tests, which allows for high strain rates. The tests were carried out using RSO type rotary flywheel impact hammer manufactured by WPM Leipzig (Figure 2). The impactor's linear velocity of 4, 7 and 14.5 m/s corresponded to the strain rate of $\dot{\varepsilon}$ = 250, 500 and 1000 s^{-1}, respectively. The force measurement methodology was based on the use of a single-rod system described by Kawata [34]. The diagram of the working part of the hammer is shown in Figure 2a. The flywheel (5) have a diameter of 0.6 m and the weight equal to 230 kg. It is precisely mounted on shaft and accelerated by the electric motor to the desired rotational speed. Once the desired velocity is reached, the claw (4) is released by the electromagnetic lock and moved outwards by centrifugal force. The claw (4) hits the anvil (3) of the sample (1) which is mounted to upper holder (2) connected permanently to the receiving rod (6). The rod is equipped with a dedicated measuring system (7) consisting of 1 mm long, 120 Ω foil strain gauges (4 active strain gauges glued parallel to rod's axis every 90° and 4 strain gauges for temperature compensation above them glued perpendicularly to rod's axis) mounted at a distance equal to eight diameters of the rod from the end closer to the specimen. The selected distance guaranteed uniform distribution of axial stresses over the entire cross-section of the rod. The other end of the rod was mounted to the ceiling (8). Data was recorded at a frequency of 1 MHz.

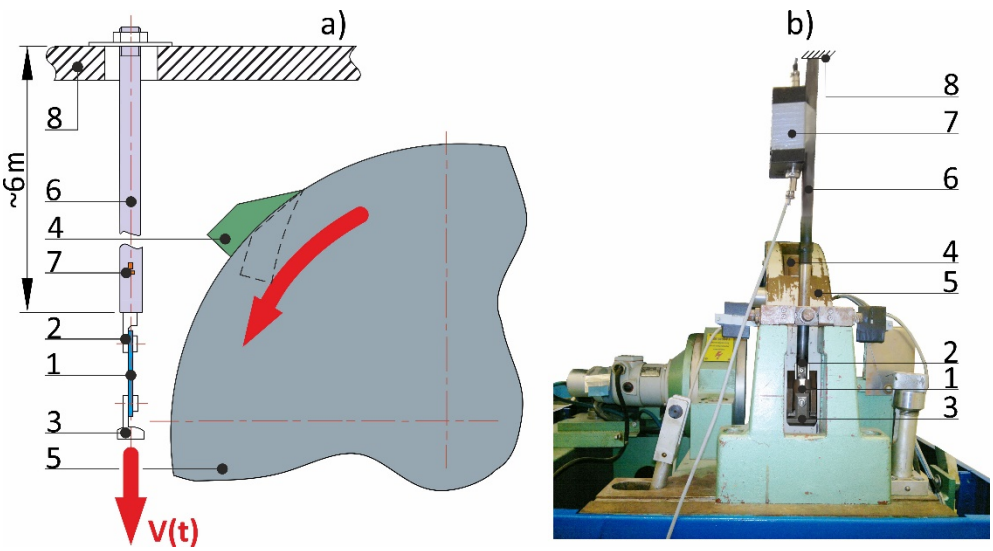

Figure 2. Rotary flywheel hammer: a) diagram of the device; b) photograph.

For each material and selected strain rate, 3–5 experiments were performed, during which force and displacement were recorded as a function of time. The obtained values were converted into engineering stress – engineering strain. The elastic part of the curves were removed, leaving only the material-plasticizing curves representing the stress to which the material must be subjected in order to continue the deformation process for a given plastic deformation.

 doi:10.20944/preprints202408.1139.v1

2.2. Testing of Energy-Absorbing Structures

2.2.1. Manufacturing

Based on the MFI index [35] and the plastic properties of the blends described in section 3.1, the specialized tools for evaluation the minimum gap ensuring its complete filling during the injection process were designed and manufactured. The tools were equipped with 25 tapered stamps and nine inlet channels. The geometry of empty space between stamps reproduced the shape of an energy-absorbing element (Figure 3). Additionally, the slot convergence angle was set to 1.78°. The slot thickness at the narrowest point where the material was to be injected at the end was only 0.1 mm. The thin-walled, energy-absorbing, honeycomb structures with a 55x55 mm cross-section and a height of 20 mm were manufactured. They had 11x11 mm pockets arranged in a 5x5 array. The height was determined basing on measurement of average height of energy-absorbing inserts made of expanded styrofoam and mounted in commercially available helmets.

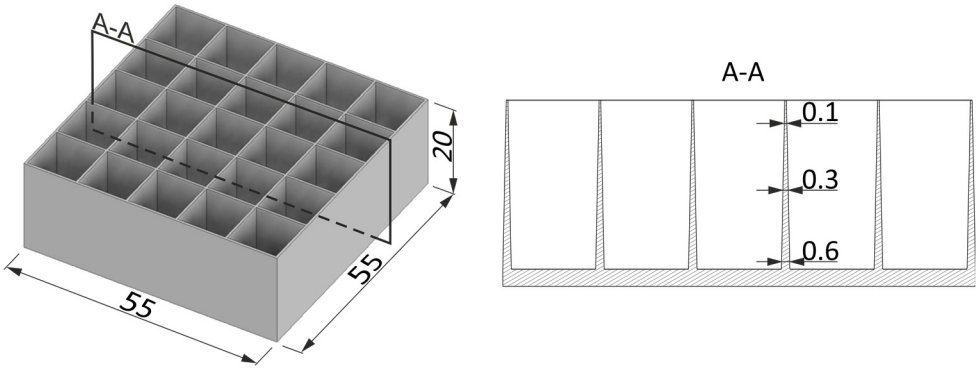

Figure 3. The geometry of energy-absorbing structures subjected to injection testing.

Based on manufacturing experience, it can be concluded that there is no chance of fully filling out the tools of described geometry. This allows to manufacture incompletely filled specimens. Based on sample measurements the impact of given manufacturing conditions (such as injection temperature, injection pressure, mold temperature) on the minimum and achievable wall thickness of the energy-absorbing insert was examined. The final design of the injection mold for producing a honeycomb structure from biodegradable plastics developed by the authors of the manuscript is subjected to patent protection at the Patent Office of the Republic of Poland (application no. P 445650 of July 21, 2023). The tools consist of 12 movable stamps and 13 stationary stamps as well as four injection points (Figure 4).

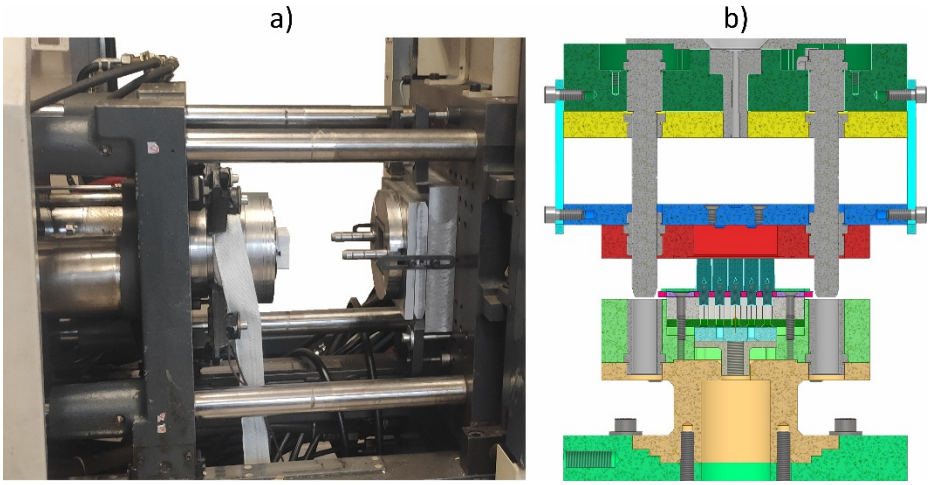

Figure 4. Injection mold used for the production of energy-absorbing structures a) tools mounted on the injection molding machine; b) cross-section of the tools - model.

 doi:10.20944/preprints202408.1139.v1

Given the very large lateral surface area of the insert, its small thickness, and the limited strength of the material, the described proprietary solution is the only way to demold the element without damaging it. The mold was mounted on a 50t Demag Ergotech Compact 50–120 injection molding machine. The technological parameters of the protective insert injection process are presented in Table 2.

Table 2. Technological parameters of the injection molding process.

Blend	PLA/PBAT blend	PLA/TPS blend
Mold temperature [°C]	50	50
Injection molding screw temperature [°C]	205-200-190-180	210-205-195-185
Injection pressure [bar]	900	950
Injection velocity [m/s]	120	120
Injection time [s]	8	8
Clamping pressure [bar]	130	130
Cooling time before opening the mold [s]	40	40
Injected volume [cm^3]	20	20

2.2.2. Crashworthiness Testing

Dynamic testing of the crashworthiness of energy-absorbing structures was performed on 9250HV Instron spring-loaded drop hammer depicted in Figure 5a. The test stand was equipped with load cell for the force signal registration (sampling rate of 82 kHz), while the VEO 710L Phantom high-speed camera combined with the dedicated image analysis software (TEMA Pro - Advanced Motion and Deformation Analysis Software) was used for the registration of the high-contrast markers located beforehand on the machines' impactor (Figure 5b) and the anvil (Figure 5c). The camera recorded files with the exposure of 32.5 µs plus 6.0 µs EDR at a resolution of 512x400 pixels (sampling rate of 31 kHz). In the next step the sampling frequencies of both signals were unified in the FlexPro software using advanced interpolation function, which allowed for creation of the final force-displacement F = f(d) graphs.

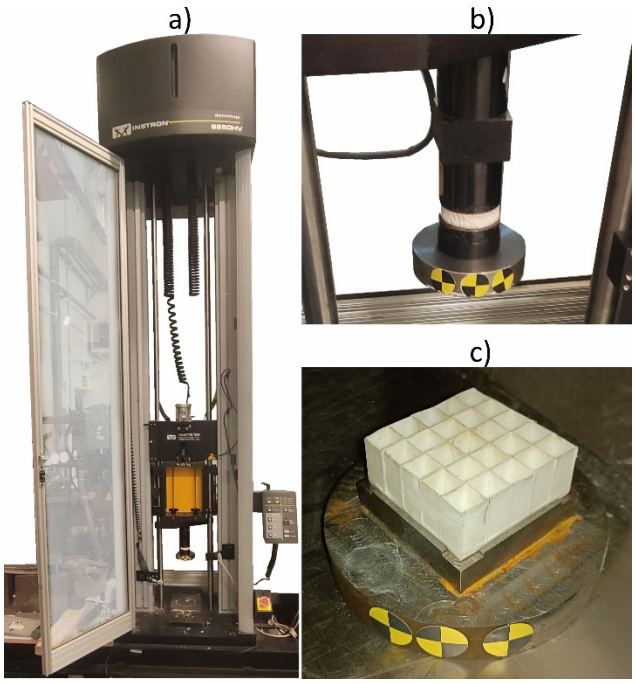

Figure 5. Spring-loaded dynamic crushing test stand - Instron 9250HV: a) general view; b) impactor's tup; c) impactor's anvil.

 doi:10.20944/preprints202408.1139.v1

As stated by the EN-1078 standard for testing bicycle helmets, a medium size headform (mass of 4.1 kg) manufactured according to EN-960 standard should be used [36]. A sport helmet should be fastened on the headform and dropped freely onto the metal base from a height of 1.5 m. The kinetic energy that should be absorbed by the protective layer of the helmet is equal to $E_k = m \cdot g \cdot h = 4.1 \cdot 9.80665 \cdot 1.5 \approx 60$ J. During an impact, the insole located directly above the fontanel (top, central part of the skull) absorbs the most of the impact energy. In order for the test conditions to be consistent with the guidelines contained in the standard all of the manufactured insert were subjected to 60 J impacts. The impactor weighing 8.412 kg was dropped freely onto the manufactured energy-absorbing structures from a height of 0.727 m ($E_k = m \cdot g \cdot h = 8.412 \cdot 9.80665 \cdot 0.727 \approx 60$ J). The impact velocity was equal to $V = (2 \cdot g \cdot h)^{0.5} \approx 3.77$ m/s.

In order to test the strain-rate influence the impact velocity of 4.88 m/s (100J) were additionally tested. To investigate the effect of the temperature on crushing force and maximum deflection of the structure the specimens were placed on the anvil located in central part of the temperature chamber (as depicted in Figure 5c). This is a very important issue due to the fact that sports helmets can be used at any time of the year, so they must be resistant to low and high temperatures. Following temperatures were tested: -20, 0, 20 and 40 °C. The temperature inside chamber were controlled with the use of additional K-type thromocouple. Second thermocouple was attached to the specimen, thus ensuring that the measured temperature is the actual temperature of the tested material.

2.3. FEM Simulation

The aim of conducting the numerical simulation is to build a material model allowing to predict accurate behavior of energy-absorbing of different of other geometries.

2.3.1. Material Model

The Young's modulus and poison's ratio were determined on the basis of quasi-static tensile tests, while the density was obtained by measuring dimensions and the mass of the cuboid, injection molded specimens. The exact values are presented in Table 3.

Table 3. Material properties of selected biodegradable blends.

Material	Young's modulus [GPa]	Poisson's ratio [-]	Density [g/mm3]
PLA15TPS85	0.24	0.22	0.00114

Biodegradable plastics are very complex and non-linear materials which mechanical properties vary depending on, among others: stress level, strain rate, and temperature. Therefore, in order to select the strain-rate sensitive model that best reflects reality, the plasticization curves presented in section 3.1 was used in order to build both Cowper-Symonds (eq. 1) and simplified Johnson-Cook (eq. 2) material models.

$$\tilde{\sigma} = \left[1 + \left(\frac{\dot{\varepsilon}}{D}\right)^{\frac{1}{p}}\right] \tag{1}$$

$$\tilde{\sigma} = (A + B \cdot \varepsilon^n) \cdot \left[1 + C \cdot ln\frac{\dot{\varepsilon}}{\dot{\varepsilon}_{st}}\right] \tag{2}$$

The quasi-static and dynamic tensile curves were converted to true stress–- true strain curves and then transformed to plasticizing curves (as depicted in Figure 8). Next, they were subjected to statistical analysis to estimate the R^2 coefficients. Next both models were used in Explicit simulation to compare crushing curves of thin-walled structures with the data gathered during experiment.

2.3.2. Boundary Conditions

The 3D solid, geometrical model of energy-absorbing structure was created using CATIA software . Next the surface model was build. The middle surfaces were then exported as IGES files

 doi:10.20944/preprints202408.1139.v1

to FEM analysis software (ABAQUS). The imported geometry was used for mesh generation (Figure 6a). The finite model consisted of 0.5 mm 4-node, quadrilateral, stress/displacement shell elements (S4R) with reduced integration and a large-strain formulation.

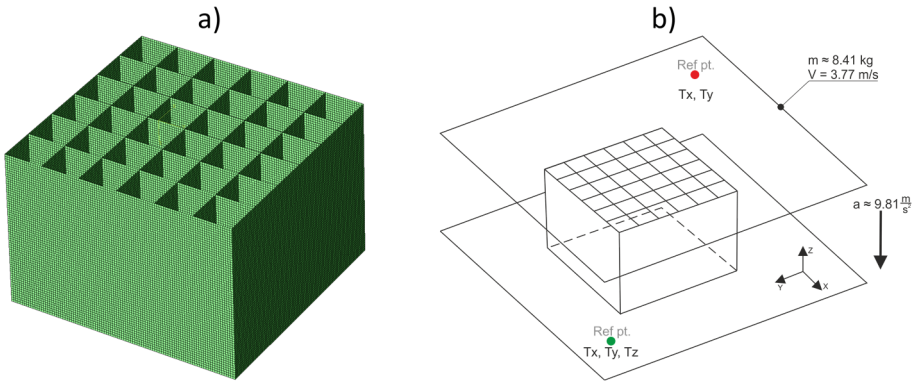

Figure 6. FEM model of the energy-absorbing protective insert a) mesh, b) boundary conditions.

The tested protective insert was supported at the bottom by a steel, fixed plate (TX, TY, TZ) of an infinite stiffness. The specimens were positioned on the top of bottom plate. The friction coefficient of 0.3 was assigned. The drop hammer's tup used during experiment was guided, allowing only movement in the vertical direction. Therefore, the tup was represented as a rigid, upper plate of an infinite stiffness with only one degree of freedom (TZ). The stiffness of the support and the tup was much greater than the stiffness of the plastic insert, so they can be considered as perfectly rigid, without assignation of any mechanical properties. The bounduary conditions are depicted in Figure 6b.

An acceleration vector (0, 0, -9.80665) m/s² was assigned to the entire finite model. A mass of 8.412 kg was assigned to the rigid point of the upper plate, which corresponded to the mass of the tup. The mass was released from a height of 0.727 m, so the initial velocity of the falling part was set to 3.77 m/s. The energy of the entire system was equal to 60 J. This energy should be absorbed (according to the EN 1078 concerning bicycle helmets) by the entire energy-absorbing insert of a helmet. A general contact algorithm was also applied, with the possibility of separation.

3. Results

3.1. Determination of Plasticizing Curves

Engineering stress – engineering strain plasticizing curves (without elastic range) collected during quasi-static and dynamic tensile tests are shown in the Figure 7a-c (PLA/PBAT mixtures) and in the Figure 7d-f (PLA/PBS mixtures). To increase the readability of the graph, only 1 representative curve is presented for each strain rate. Irregular oscillations of the curves recorded during dynamic testing results from the reflection of the elastic wave from the end of the rod that is attached to the ceiling.

Irrespectively of the tested material, the significant difference between static and dynamic testing conditions may be observed. First, the significant, positive strain-rate sensitivity was observed. The intensity of this effect was strongly dependent on the amount of softening additive (PBAT or TPS). In the case of 50% of addition the ratio of dynamic yield strength to quasi-static yield strength was varying from 1.5 (for PLA50PBAT50) to 1.73 (for PLA50TPS50). As the amount of softening additive increases, the coefficient increases too. When the amount of softening additive reaches 85%, the after mentioned coefficient it is equal to 2.5 (for PLA15PBAT85) and 3.1 (for PLA15TPS85).

 doi:10.20944/preprints202408.1139.v1

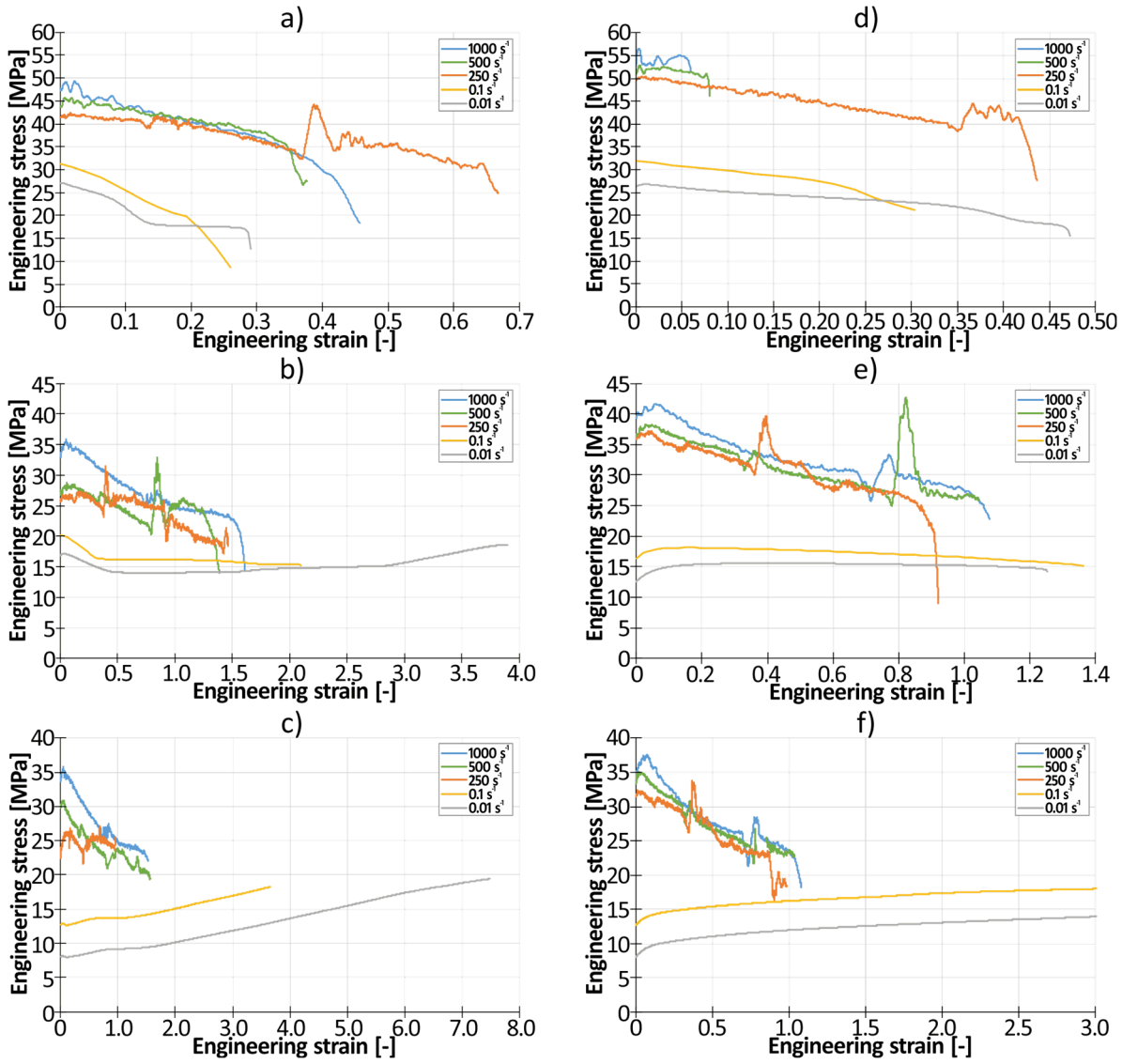

Figure 7. Engineering stress – engineering strain plasticizing curves of tested materials: a) PLA50PBAT50; b) PLA30PBAT70; c) PLA15PBAT85; d) PLA50TPS50; e) PLA30TPS70; f) PLA15TPS85;.

It may be also observed that there is significant influence of the softening additive on the plastic properties of the blend in quasi-static conditions. Increase of the softening agent from 50% to 85% results in the significant increase of elongation at break from 0.025 (for PLA50PBAT50; $\dot{\varepsilon}$=0.01) and 0.35 (for PLA50TPS50; $\dot{\varepsilon}$=0.01) to about 3.7 (for PLA18PBAT80; $\dot{\varepsilon}$=0.01) and 3.0 (for PLA15TPS85; $\dot{\varepsilon}$=0.01).

Moreover, character of the stress-strain curve is also influenced by the amount of pure PLA in the blend. For 50/50 blends, the quasi-static stress-strain curves have always descending character. The decrease of PLA to 30% results in almost constant level of tensile stress throughout the test until failure. In the case of mixtures containing only 15% of PLA the curves were always monotonically increasing until the failure occurred.

3.2. Testing of Energy-Absorbing Structures

3.2.1. Manufacturing

The walls of the energy-absorbing structures obtained during injection tests were measured in 10, randomly selected thinnest cross-section located at the top, as shown in Figure 8. Next, the average

 doi:10.20944/preprints202408.1139.v1

value was calculated. In this way, the minimum gap that could be filled by particular blends of biodegradable plastics was determined. The measured values are presented in Table 5.

Figure 8. Location of measuring points for calculation of minimal thickness that can be successfully injection molded.

In the case of both tested combination of materials, it can be concluded that the increase in the percentage of plasticizing additive (PBAT or TPS) in the blend results in decrease of the thickness of the gap that can be successfully filled during injection molding (Table 4). Increasing the plasticizing additive by 35% (from 50% to 85%) results in decrease of the thicknees of the gap by about 32% in the case of PLA/PBAT blends (from 0.22 mm to 0.15 mm) and by about 26% in the case of PLA/TPS blends (from 0.23 mm to 0.17 mm).

Table 4. The value of the minimum gap that can be filled by the tested materials.

Material (PBAT blends)	Minimal gap [mm]	Material (TPS blends)	Minimal gap [mm]
PLA50PBAT50	0.22 ± 0.01	PLA50TPS50	0.23± 0.01
PLA30PBAT70	0.18 ± 0.02	PLA30TPS70	0.20 ± 0.02
PLA15PBAT85	0.15 ± 0.01	PLA15TPS85	0.17 ± 0.02

3.2.2. Crashworthiness Testing

Force-deflection graphs obtained during the dynamic crushing tests of the ready-made specimens at a room temperature were depicted in Figure 9. The crushing curve of expanded polystyrene cut out from a commercially available bike helmet was presented as a reference.

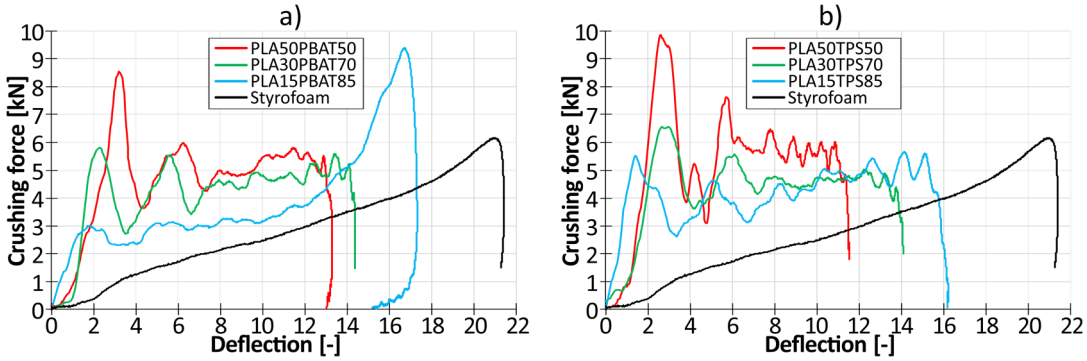

Figure 9. Force-deflection graphs of inserts made of blends based on a) PLA and PBAT; b) PLA and TPS.

Analyzing the force-displacement curves in Figure 9, it can be observed that during dynamic crushing of the designed protective inserts made of bioplastics, there is a large and unfavorable, force peak at the beginning of the graph, especially for materials of a higher content of PLA. This is due to

 doi:10.20944/preprints202408.1139.v1

the high initial resistance of the structure, which is much stiffer than an insert made of expanded polystyrene. The subsequent oscillations of the curves are related to the formation of a plastic folds, which is the most effective energy absorption mechanism. This is evidenced by the fact that the 60 J impact was absorbed by most of the tested inserts through an 11 - 14 mm deflection of the insert which is over 40% smaller than in the case of a styrofoam insert (21 mm deflection).

The final increase in the force value on the styrofoam curve is related to the maximum and complete compression of the insert, which is associated with a high risk of complete crushing of the energy-absorbing elements. This includes, especially for impact of a higher energy than defined in the standards, increased head injuries caused by contact of the users' head with a hard outer shell. It can be observed that as the content of plastic PBAT or TPS increases, the curve's oscillations are reduced, and the curves begin to resemble the styrofoam crushing curve.

The obtained values of the maximum deflection of structures and the maximum overload (g-force) that was registered for each of the tested material were accordingly shown in Figure 10. The trend line for individual blends was additionally marked with a dashed line.

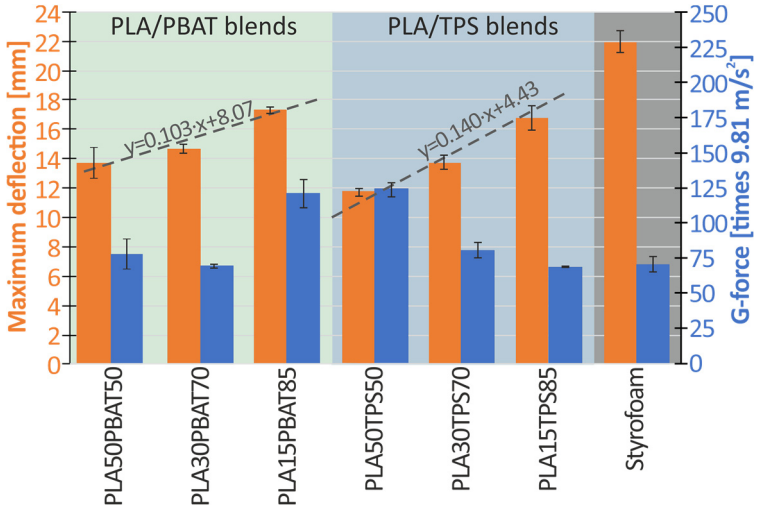

Figure 10. A graph of maximum deformation of the inserts and maximum overload occurring during crushing.

Based on Figure 10 (blue bars), it can be observed that none of the tested materials (biodegradable or polystyrene) exceeded the maximum permissible values defined by EN 1078 standard (250 g, which for a impactor's mass of 8.412 kg, results in 20.6 kN).

Comparing PLA/PBAT blends to the reference styrofoam (deceleration of 74g and the maximum deflection of 21.3mm), the PLA50PBAT50 blend was characterized by 15% higher g-force but 38% lower deflection. The PLA30PBAT70 had nearly the same g-force, but still about 33% lower deflection, while the PLA15PBAT85 blend proved to have 54% higher acceleration level and only about 19% lower deflection. When it comes to comparison of PLA/TPS blends with the styrofoam, the PLA50TPS50 blend was the worst one, reaching about 64% higher g-force. The most promising materials were PLA30TPS70 (35% lower deflection; 10% higher g-force) and PLA15TPS85 (24% lower deflection; 10% lower g-force). Due to the very large force peak occurring in the initial stage of crushing the PLA50PBAT50 and PLA50TPS50 inserts, they were excluded from further research work. Such high force peak at the beginning of an impact may cause discomfort and result in increased injuries to the user of a helmet equipped with such protective insert.

For the remaining materials: PLA30PBAT70, PLA15PBAT85, PLA30TPS70 and PLA15TPS85, crushing tests were performed using a temperature chamber to examine the effect of temperature on energy absorption and maximum deflection of the structure. The results in the form of a scatter chart are shown in Figure 11. The average force for the deflection of 12 mm is marked in orange, while the maximum deflection after absorbing the entire impact energy (60 J) is marked in blue.

 doi:10.20944/preprints202408.1139.v1

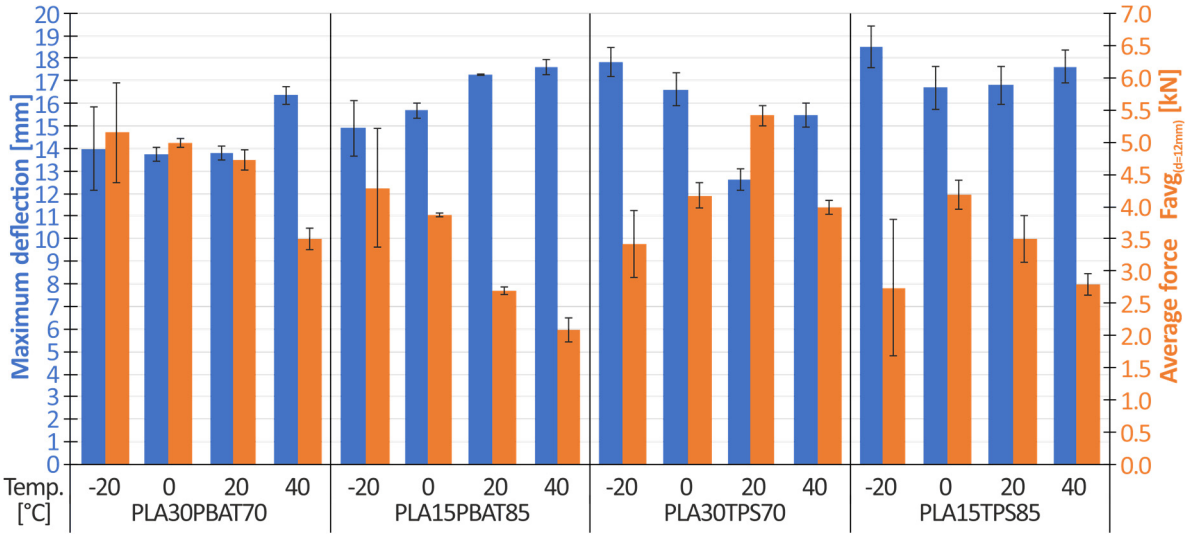

Figure 11. The influence of temperature on the average force (at a deflection of 12 mm) and on the maximum deflection of the energy-absorbing structures.

Analysing figure 11, the following conclusions were drawn:

1. There is a clear influence of the amount of plasticizer in the case of PLA/PBAT mixtures. The PLA15PBAT85 mixture have a deflection greater by approximately 7% (for T = -20°C), 14% (for T = 0°C), 25% (for T = 20°C), and 8% (for T = 40° C) relative to the PLA30PBAT70 mixture. For both mixtures, the maximum deflection increases as the material temperature increases.
2. Samples made of the PLA30PBAT70 mixture achieve a higher value of the average crushing force $Favg_{(d = 12\ mm)}$ at a deflecion of 12 mm, compared to samples made of the PLA15PBAT85 material. The differences intensify as the temperature increases. The ratio of the average force $Favg_{(d = 12\ mm)}$ of the PLA30PBAT70 material to the average force $Favg_{(d = 12\ mm)}$ of the PLA15PBAT85 material is respectively: 1.21 (for T = -20°C), 1.35 (for T = 0°C), 1.75 (for T = 20°C), and 1.59 (for T = 40°C).
3. Different characteristics of TPS and PBAT softening additives were noticed. In the case of temperatures ranging from -20°C to 0°C, comparing the same amount of TPS and PBAT additives (PLA30TPS70 vs. PLA30PBAT70 and PLA15TPS85 vs. PLA15TBAT85), materials with the addition of TPS have several percent greater deflection and a lower value of the average crushing force $Favg_{(d = 12\ mm)}$ compared to materials based on PBAT. In the case of temperatures ranging from 20°C to 40°C, the opposite situation occurs: materials with the addition of TPS are characterized by lower maximum deflection and greater crushing force.

On the basis of visual inspection of the deformation mode, all of the PLA/TPS blends were rejected. Specimens made of those blends were cracking brittely independently of the amount of TPS addition, which is depicted in Figure 12.

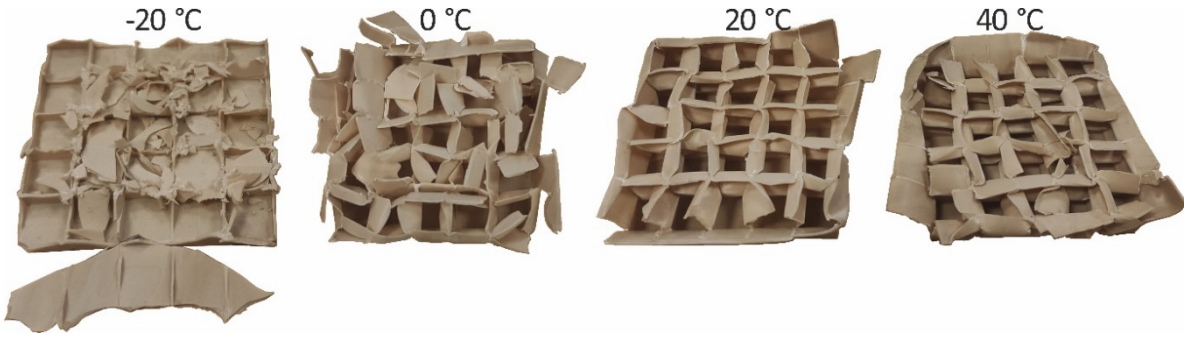

Figure 12. Typical crushing mode of PLA30TPST70 and PLA15TPS85.

 doi:10.20944/preprints202408.1139.v1

The PLA30PBAT70 and PLA15PBAT85 blends were selected as the most promising ones in terms of further use as the energy absorbing liner in bicycle helmets. In order to check strain rate influence of selected blends, two different impact velocities were applied: 3.77 m/s (60 J) and 4.88 m/s (100 J). The average crushing force – deflection curves are depicted in Figure 13, while pivot table presenting average crushing force at a deflection of 7 mm $Favg_{(d=7\,mm)}$ and maximum deflection is presented in Figure 14.

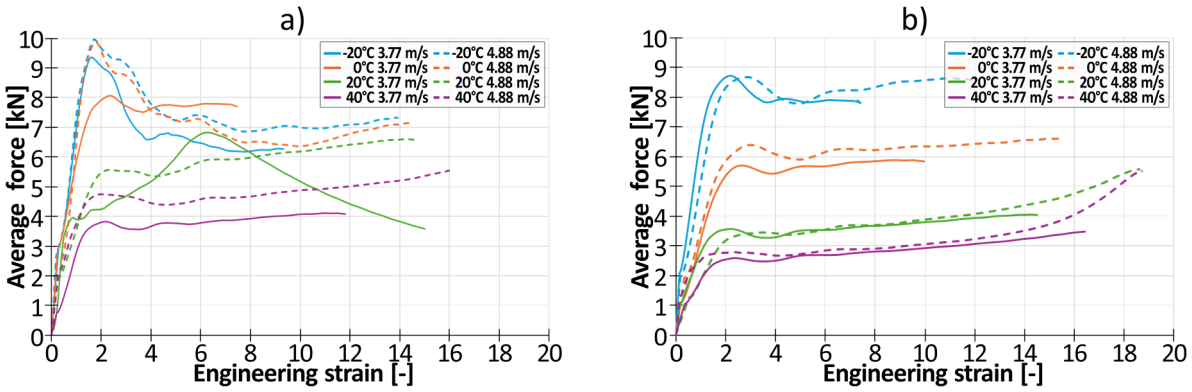

Figure 13. Average crushing force – deflection of selected structures a) PLA30PBAT70, b) PLA15PBAT85.

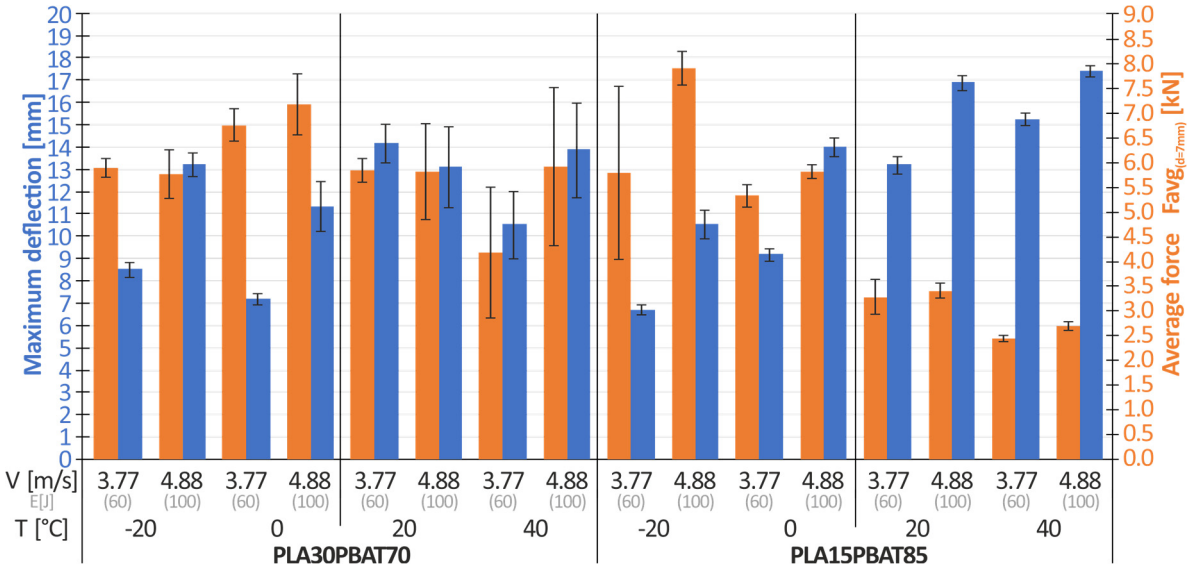

Figure 14. The influence of temperature on the average force (at a deflection of 7 mm) and on the maximum deflection of the energy-absorbing structures.

Based on Figure 14, it can be observed that as the impact velocity increases, the value of the average crushing force $Favg_{(d=7\,mm)}$ and the maximum deflection of the sample increase. The exception is the PLA30PBAT70 blend crushed at -20 °C and 20 °C. The average increase of the average crushing force for both materials (for all temperatures) was 13%, while the average increase in the maximum deflection was 36%. This is a very favorable phenomenon proving that the material is not sensitive to the strain rate, and therefore that the material remain similar stiffness as the impact velocity increases. The increased amount of energy is absorbed by the increased deflection of the insert. Due to this, the increased impact velocity does not cause a proportional increase in head injuries to the user of the helmet equipped with the tested inserts and it remains at a similar level despite the increase in the impact energy from 60J to 100J, which is a value higher by 66% than the load defined by the EN 1078 standard for testing sports helmets.

 doi:10.20944/preprints202408.1139.v1

The deformation mode of the samples is depicted in Figure 15. It can be seen that the PLA30PBAT70 material at negative temperatures has a high tendency to disintegration associated with defragmentation at -20°C.

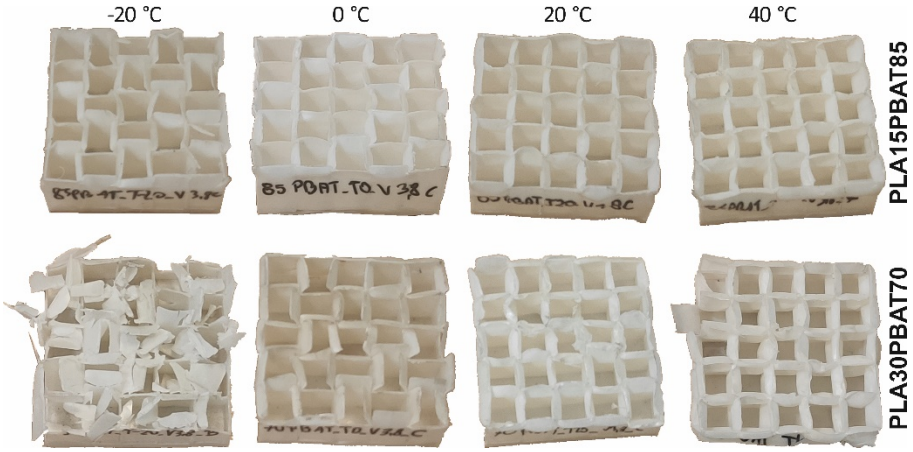

Figure 15. The influence of temperature on the deformation mode of specimens impact velocity of 3.77 m/s.

Moreover, at sub-zero temperatures a large initial force peak is present, which results from higher initial stiffness of undeformed material. After initiation of folding process the force value drops almost to 0 (Figure 16), which induces brittle cracking. This phenomenon was not observed in the case of the PLA15PBAT85 mixture. The registered values force oscillate have also about 30-50% lower oscillations. Therefore PLA15PBAT85 is recommended for further development in sport helmets.

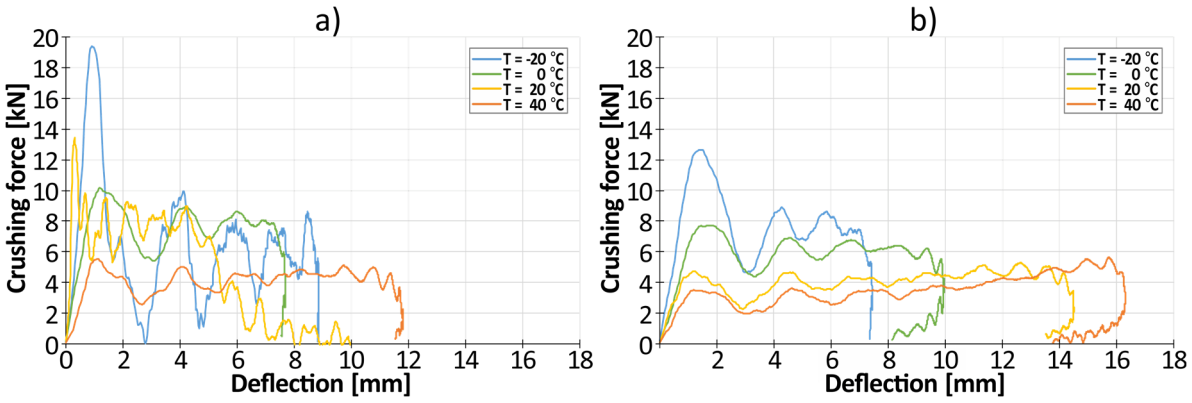

Figure 16. The influence of temperature on crushing force – displacement curves of: a) PLA30PBAT70; b) PLA15PBAT85.

3.3. FEM Simulation

3.3.1. Materials Model

Based on data recorded during quasi-static and dynamic tensile tests of injected dog-bone specimens, material models taking into account strain rate sensitivity (Cowper-Symonds model and simplified Johnson-Cook model) were developed for the PLA15PBAT85. The fit of the resulting Cowper-Symonds models and the simplified Johnson-Cook model to the data obtained by measurement is presented in Figure 17.

Preprints.org (www.preprints.org) | NOT PEER-REVIEWED | Posted: 15 August 2024 doi:10.20944/preprints202408.1139.v1

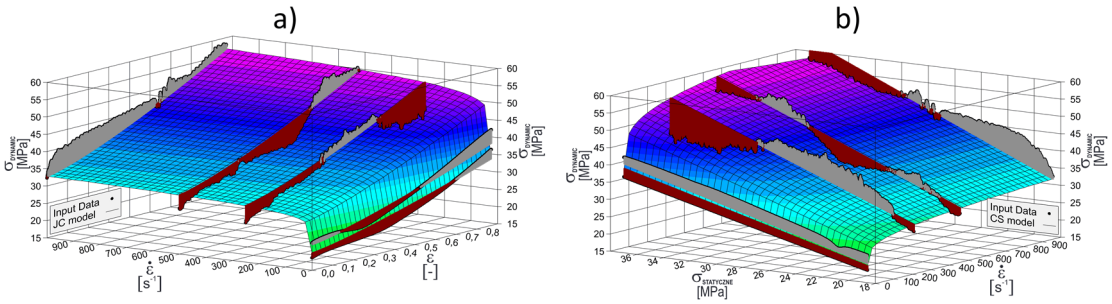

Figure 17. Correlation of the material models to the experimental data: a) Johnson-Cook simplified; b) Cowper-Symonds.

As a result of the analysis, the crucial parameters of both material models were estimated. The statistical data was also analyzed, in particular the correlation coefficient R^2 and confidence intervals for the significance level $\alpha = 0.05$ (95% confidence level). All of the data is presented in Table 5.

Table 5. Crucial coefficients of material models.

PLA15PBAT85 material model	Param.	Value [-]	σ [-]	Value [-]	R^2 [-]
Cowper-Symonds $\tilde{\sigma} = \left[1 + \left(\frac{\dot{\varepsilon}}{D}\right)^{\frac{1}{p}}\right]$	D	5647	$D_{0.95}$	±432	0.88
	p	4,85	$p_{0.95}$	±0,14	
Johnson-Cook simpl. $\tilde{\sigma} = (A + B \cdot \varepsilon^n) \cdot \left[1 + C \cdot ln\frac{\dot{\varepsilon}}{\dot{\varepsilon}_{st}}\right]$	A	19.90	$A_{0.95}$	±0.21	0.92
	B	17.27	$B_{0.95}$	±0.23	
	C	0.0565	$C_{0.95}$	±0.0008	
	n	1.2601	$n_{0.95}$	±0.0451	

The material models are characterized by a correlation coefficient R^2 of around 0.9 which indicates a good fit of the measurement data to the constitutive equations of the models. The simplified Johnson-Cook material model provides a much better fit than the Cowper-Symonds material model. Therefore, it is recommended to use the simplified Johnson-Cook model for the selected blend.

3.3.2. Numerical Simulation of Dynamic Compression Test of Energy-Absorbing Structure

A comparison of the final deformation mode obtained after dynamic crushing to the FE simulation was depicted in Figure 18, whereas the force – deflection curves are presented in Figure 18b.

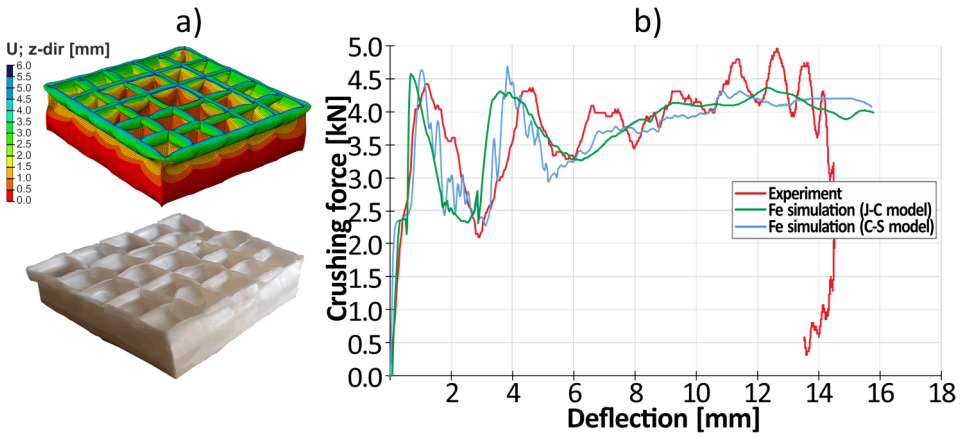

Figure 18. Comparison of the simulation and the crushing experiment (dynamic conditions) a) deformation mode; b) crushing force – deflection curve.

 doi:10.20944/preprints202408.1139.v1

The simulations turned out to be consistent with the experiment. The construction of the model and numerical simulation allows testing geometric parameters such as the shape of the mesh, wall thickness and height of the structure. The developed numerical simulation allows with high probability to determine the optimal geometric parameters, including the appropriate ratio of wall thickness to the height of the structure, which will prevent global buckling and allow for the plastic folding, which is one of the most effective energy absorption mechanism. No significant differences were spotted between the use of Johnson-Cook and Cowper-Symonds material models.

4. Summary

To sum up, based on the results obtained from experimental tests and numerical simulations, the following conclusions can be drawn:

1. In the case of materials' mechanical properties, the significant, positive strain-rate sensitivity was observed. The intensity of this effect was strongly dependent on the amount of softening additive (PBAT or TPS). In the case of 50% of addition the ratio of dynamic yield strength to quasi-static yield strength was varying from 1.5 (for PLA50PBAT50) to 1.73 (for PLA50TPS50). As the amount of softening additive increases, the coefficient increases to 2.5 (for PLA15PBAT85) and 3.1 (for PLA15TPS85). Increase of the softening agent from 50% to 85% results in the significant increase of elongation at break from 0.025 (for PLA50PBAT50; $\dot{\varepsilon}$=0.01) and 0.35 (for PLA50TPS50; $\dot{\varepsilon}$=0.01) to about 3.7 (for PLA18PBAT80; $\dot{\varepsilon}$=0.01) and 3.0 (for PLA15TPS85; $\dot{\varepsilon}$=0.01).
2. There is a clear influence of the amount of plasticizer in the case of PLA/PBAT energy-absorbing structures. The PLA15PBAT85 mixture have a deflection greater by approximately 7% (for T = -20°C), 14% (for T = 0°C), 25% (for T = 20°C), and 8% (for T = 40° C) relative to the PLA30PBAT70 mixture. For both mixtures, the maximum deflection increases as the material temperature increases.
3. Both Johnson-Cook and Cowper-Symonds material models are in good agreement with the experiment. This allows for further prediction of optimal geometric parameters of energy-absorbing structures on the basis of FE simulations.
4. In the case of both tested combination of materials, it can be concluded that the increase in the percentage of plasticizing additive (PBAT or TPS) in the blend results in decrease of the thickness of the gap that can be successfully filled during injection molding (Table 5). Increasing the plasticizing additive by 35% (from 50% to 85%) results in decrease of the thickness of the gap by about 32% in the case of PLA/PBAT blends (from 0.22 mm to 0.15 mm) and by about 26% in the case of PLA/TPS blends (from 0.23 mm to 0.17 mm).
5. As the content of plastic PBAT or TPS increases, the curve becomes flatter, i.e. the amplitude representing formation of the plastic folds becomes smaller, and the curves begin to resemble the styrofoam curve.

Author Contributions: Conceptualization, Paweł Kaczyński and Mateusz Skwarski; Formal analysis, Anna Dmitruk; Funding acquisition, Paweł Kaczyński; Investigation, Paweł Kaczyński, Mateusz Skwarski, Anna Dmitruk, Piotr Makuła and Joanna Ludwiczak; Methodology, Paweł Kaczyński, Mateusz Skwarski and Piotr Makuła; Resources, Joanna Ludwiczak; Validation, Anna Dmitruk and Piotr Makuła; Visualization, Paweł Kaczyński; Writing – original draft, Paweł Kaczyński and Mateusz Skwarski; Writing – review & editing, Anna Dmitruk, Piotr Makuła and Joanna Ludwiczak.

Funding: This research was funded by THE NATIONAL CENTRE FOR RESEARCH AND DEVELOPMENT (NCBiR, Poland), grant number 0223/L-11/2019, LIDER

Conflicts of Interest: The authors declare no conflicts of in-terest. The funders had no role in the design of the study; in the collection, analyses, or interpretation of data; in the writing of the manuscript; or in the decision to publish the results.

 doi:10.20944/preprints202408.1139.v1

References

1. Ha, N.S.; Lu, G. A Review of Recent Research on Bio-Inspired Structures and Materials for Energy Absorption Applications. Compos. Part B Eng. 2020, 181, 107496, doi:10.1016/j.compositesb.2019.107496.
2. Yang, S.; Bieliatynskyi, A.; Trachevskyi, V.; Shao, M.; Ta, M. Technology for Improving Modern Polymer Composite Materials. Mater. Sci. Pol. 2022, 40, 27–41, doi:10.2478/msp-2022-0027.
3. Czech, K.; Oleksy, M.; Oliwa, R.; Domańska, A. Hybrid Polymer Composites with Enhanced Energy Absorption. Polimery/Polymers 2022, 67, 552–560, doi:10.14314/polimery.2022.11.2.
4. Technical, O. Comparative Evaluation of Mechanical Properties of Short Aramid Fiber on Thermoplastic Polymers 1. 2023, 41, 161–176, doi:10.2478/msp-2023-0012.
5. Akademia Baru, P.; Sofi, M.I.M. A Review on Energy Absorption of Multi Cell Thin Walled Structure. J. Adv. Rev. Sci. Res. ISSN 2015, 16, 2289–7887.
6. Wang, X.; Wang, X.; Jian, K.; Xu, L.; Ju, A.; Guan, Z.; Ma, L. Mechanical Properties of Al Foams Subjected to Compression by a Cone-Shaped Indenter. ACS Omega 2021, 6, 28150–28161, doi:10.1021/acsomega.1c04217.
7. Endut, N.A.; Al Hazza, M.H.F.; Sidek, A.A.; Adesta, E.T.Y.; Ibrahim, N.A. Compressive Behaviour and Energy Absorption of Aluminium Foam Sandwich. IOP Conf. Ser. Mater. Sci. Eng. 2018, 290, 2–7, doi:10.1088/1757-899X/290/1/012084.
8. Mahajan, A.; Singh, G.; Devgan, S. Additive Manufacturing of Metallic Biomaterials: A Concise Review. Arch. Civ. Mech. Eng. 2023, 23, 1–15, doi:10.1007/s43452-023-00730-7.
9. Puga, H.; Carneiro, V.H.; Correira, P.; Vieira, V.; Barbosa, J.; Meireles, J. Mechanical Behavior of Honeycomb Lattices Manufactured by Investment Casting for Scaffolding Applications. Proc. Inst. Mech. Eng. Part L J. Mater. Des. Appl. 2016, 231, 73–81, doi:10.1177/1464420716665414.
10. Rahman, O.; Koohbor, B. Optimization of Energy Absorption Performance of Polymer Honeycombs by Density Gradation. Compos. Part C Open Access 2020, 3, 100052, doi:10.1016/j.jcomc.2020.100052.
11. Ingrole, A.; Aguirre, T.G.; Fuller, L.; Donahue, S.W. Bioinspired Energy Absorbing Material Designs Using Additive Manufacturing. J. Mech. Behav. Biomed. Mater. 2021, 119, 104518, doi:10.1016/j.jmbbm.2021.104518.
12. Doodi, R.; Gunji, B.M. Prediction and Experimental Validation Approach to Improve Performance of Novel Hybrid Bio-Inspired 3D Printed Lattice Structures Using Artificial Neural Networks. Sci. Rep. 2023, 13, 1–17, doi:10.1038/s41598-023-33935-0.
13. Belingardi, G.; Montanini, R.; Avalle, M. Characterization of Polymeric Structural Foams under Compressive Impact Loading by Means of Energy-Absorption Diagram. Int. J. Impact Eng. 2001, 25, 455–472.
14. Khatri, N.R.; Egan, P.F. Energy Absorption of 3D Printed ABS and TPU Multimaterial Honeycomb Structures. 3D Print. Addit. Manuf. 2023, 11, e840–e850, doi:10.1089/3dp.2022.0196.
15. Kumar, A.; Collini, L.; Ursini, C.; Jeng, J.Y. Energy Absorption and Stiffness of Thin and Thick-Walled Closed-Cell 3D-Printed Structures Fabricated from a Hyperelastic Soft Polymer. Materials (Basel). 2022, 15, doi:10.3390/ma15072441.
16. Namvar, N.; Zolfagharian, A.; Vakili-Tahami, F.; Bodaghi, M. Reversible Energy Absorption of Elasto-Plastic Auxetic, Hexagonal, and AuxHex Structures Fabricated by FDM 4D Printing. Smart Mater. Struct. 2022, 31, doi:10.1088/1361-665X/ac6291.
17. Günaydın, K.; Rea, C.; Kazancı, Z. Energy Absorption Enhancement of Additively Manufactured Hexagonal and Re-Entrant (Auxetic) Lattice Structures by Using Multi-Material Reinforcements. Addit. Manuf. 2022, 59, doi:10.1016/j.addma.2022.103076.
18. Kumar, S.; Ubaid, J.; Abishera, R.; Schiffer, A.; Deshpande, V.S. Tunable Energy Absorption Characteristics of Architected Honeycombs Enabled via Additive Manufacturing. ACS Appl. Mater. Interfaces 2019, 11, 42549–42560, doi:10.1021/acsami.9b12880.
19. Mehrpouya, M.; Edelijn, T.; Ibrahim, M.; Mohebshahedin, A.; Gisario, A.; Barletta, M. Functional Behavior and Energy Absorption Characteristics of Additively Manufactured Smart Sandwich Structures. Adv. Eng. Mater. 2022, doi:10.1002/adem.202200677.
20. Ha, N.S.; Pham, T.M.; Tran, T.T.; Hao, H.; Lu, G. Mechanical Properties and Energy Absorption of Bio-Inspired Hierarchical Circular Honeycomb. Compos. Part B Eng. 2022, 236, 109818, doi:10.1016/j.compositesb.2022.109818.

21. Wu, C.; Nguyen-van, V.; Tran, P. Materials Science in Additive Manufacturing Energy Absorption and Recoverability of Moore. 2023, 2.
22. Peixinho, N.; Carvalho, O.; Areias, C.; Pinto, P.; Silva, F. Compressive Properties and Energy Absorption of Metal-Polymer Hybrid Cellular Structures. Mater. Sci. Eng. A 2020, 794, 139921, doi:10.1016/j.msea.2020.139921.
23. Diamantopoulou, M.; Roth, C.; Tancogne-Dejean, T.; Lauener, C.; Mohr, D. Ceramic/Polymer Microlattices: Increasing Specific Energy Absorption through Sandwich Construction. Extrem. Mech. Lett. 2022, 53, 101708, doi:10.1016/j.eml.2022.101708.
24. Nian, Y.; Wan, S.; Zhou, P.; Wang, X.; Santiago, R.; Li, M. Energy Absorption Characteristics of Functionally Graded Polymer-Based Lattice Structures Filled Aluminum Tubes under Transverse Impact Loading. Mater. Des. 2021, 209, doi:10.1016/j.matdes.2021.110011.
25. Chen, J.; Li, E.; Liu, W.; Mao, Y.; Hou, S. Sustainable Composites with Ultrahigh Energy Absorption from Beverage Cans and Polyurethane Foam. Compos. Sci. Technol. 2023, 239, 110047, doi:10.1016/j.compscitech.2023.110047.
26. Ragab, A.M.; Mahdi, E.; Oosterhuis, K.; Dean, A.; Cabibihan, J.J. Mechanical and Energy Absorption Properties of 3D-Printed Honeycomb Structures with Voronoi Tessellations. Front. Mech. Eng. 2023, 9, 1–15, doi:10.3389/fmech.2023.1204893.
27. Shevchenko, V.; Balabanov, S.; Sychov, M.; Karimova, L. Prediction of Cellular Structure Mechanical Properties with the Geometry of Triply Periodic Minimal Surfaces (TPMS). ACS Omega 2023, 8, 26895–26905, doi:10.1021/acsomega.3c01631.
28. Gisario, A.; Desole, M.P.; Mehrpouya, M.; Barletta, M. Energy Absorbing 4D Printed Meta-Sandwich Structures: Load Cycles and Shape Recovery. Int. J. Adv. Manuf. Technol. 2023, 127, 1779–1795, doi:10.1007/s00170-023-11638-0.
29. Bolan, M.; Dean, M.; Bardelcik, A. The Energy Absorption Behavior of 3D-Printed Polymeric Octet-Truss Lattice Structures of Varying Strut Length and Radius. Polymers (Basel). 2023, 15, doi:10.3390/polym15030713.
30. kumar Gurajala, N.; Sanjeev, L.; Teja, B.; Sai Kumar, T.; Eswara Manikanta, J. An Overview of Mechanical Properties of Biodegradable Polymers and Natural Fibre Materials. Mater. Today Proc. 2023, doi:10.1016/j.matpr.2023.05.161.
31. Dicks, J.A.; Woolard, C. Biodegradable Polymeric Foams Based on Modified Castor Oil, Styrene, and Isobornyl Methacrylate. Polymers (Basel). 2021, 13, doi:10.3390/polym13111872.
32. Andena, L.; Caimmi, F.; Leonardi, L.; Nacucchi, M.; De Pascalis, F. Compression of Polystyrene and Polypropylene Foams for Energy Absorption Applications: A Combined Mechanical and Microstructural Study. J. Cell. Plast. 2019, 55, 49–72, doi:10.1177/0021955X18806794.
33. Murray, C.M.; Mao, M.; Park, J.; Howard, J.; Wereley, N.M. Visco-Elastic Honeycomb Structures with Increased Energy Absorption and Shape Recovery Performance Using Buckling Initiators. Polymers (Basel). 2023, 15, doi:10.3390/polym15163350.
34. Kawata, K.; Shioiri, J. Macro-and Micro-Mechanics of High Velocity Deformation and Fracture: IUTAM Symposium on MMMHVDF Tokyo, Japan, August 12–15, 1985; Springer Science & Business Media, 2012; ISBN 3642827675.
35. Dmitruk, A.; Ludwiczak, J.; Skwarski, M.; Makuła, P.; Kaczyński, P. Influence of PBS, PBAT and TPS Content on Tensile and Processing Properties of PLA-Based Polymeric Blends at Different Temperatures. J. Mater. Sci. 2023, 58, 1991–2004, doi:10.1007/s10853-022-08081-z.
36. Emsley, B.; Farmer, J.; Sherratt, P.; Goodall, P.; Jackson, T.; West, A. An Overview of the Test Methodology Used in Current Cycling Helmet Standards and Literature. Int. J. Impact Eng. 2024, 188, 104928, doi:10.1016/j.ijimpeng.2024.104928.